



Cite this: DOI: 10.1039/d0re00129e

Received 2nd April 2020,
Accepted 26th April 2020

DOI: 10.1039/d0re00129e

rsc.li/reaction-engineering

An automated flow chemistry platform to decouple mixing and reaction times†

Robert W. Epps, Amanda A. Volk, Kameel Abdel-Latif and Milad Abolhasani *

Although a vital parameter in many colloidal nanomaterial syntheses, precursor mixing rates are typically inconsistent in batch processes and difficult to separate from reaction time in continuous flow systems. Here, we present a flow chemistry platform that decouples early-stage precursor mixing rates from reaction time (residence time) using solely off-the-shelf, commercially available, and standard dimension components. We then utilize the developed flow chemistry platform towards time- and material-efficient studies of the mass transfer-controlled synthesis of cesium lead bromide perovskite quantum dots.

Batch (*i.e.*, flask-based) reactors have long been the standard means of studying solution-phase chemical processes. But batch systems, due to their irreproducible and constrained mixing rates, are not suitable for fundamental and applied studies of mass transfer-limited processes.^{1–3} Consequently, flask-based experimental strategies are subject to substantial batch-to-batch variability and unpredictable scale-up in the colloidal synthesis of various nanomaterials.^{4,5} In contrast, flow-based synthesis platforms offer more consistent and controllable mixing rates, making them conducive for large scale manufacturing through numbered-up parallel flow reactors. Additional advantages of flow-based synthesis include superior sampling rates, access to process automation, and lower chemical consumption.^{6,7} As a subset of these flow systems, fluoropolymer tubing-based microfluidic strategies have recently emerged as a low-cost, modular, and dimensionally standardized alternative to chip-based devices for accelerated investigations of colloidal nanomaterials.⁸

In basic laminar flow synthesis systems (*i.e.*, single phase, continuous flow in an unmodified linear channel), mass

transfer rates are dependent on microchannel dimensions and fluid velocity. These diffusion limited systems offer limited mixing rates, and consequently microscale mixing enhancement strategies are required. Over the last two decades, a wide range of passive^{9,10} and active¹¹ micromixers, as well as multi-phase flow formats^{12–15} have been developed in both chip- and tube-based flow platforms. While these strategies greatly enhance fluid mixing rates, advection rates are still coupled to the average fluid velocity (and residence times) within the microchannel.

Recently, several flow synthesis strategies, including mobile non-invasive sampling methods^{16–18} and single-droplet flow reactors^{19–26} have been developed to decouple precursor mixing and reaction times. Despite the unique advantages of these flow chemistry approaches, they possess limitations in either their minimum achievable mixing time, minimum measurable residence time, or the extent to which the precursor mixing time and reaction time can be decoupled. These challenges in existing flow chemistry platforms impair our understanding of ultrafast (mass transfer-limited) reaction mechanisms and mass transfer-tuned colloidal synthesis processes.

In this work, we present an automated, modular fluidic microprocessor that can simultaneously attain arbitrarily long residence times as well as microscale precursor mixing times spanning 53 ms to 7.3 s. The developed flow chemistry platform features a passive micromixer segment and is comprised entirely of modular components with off-the-shelf parts for ease of access.

We study the performance of the developed passive micromixer to enable on-demand tuning of precursor mixing time. Through these studies, we have demonstrated complete precursor mixing for systems with Reynolds numbers ranging from 2.8 to 370. We then apply the developed time- and material-efficient flow chemistry platform towards the synthesis of colloidal perovskite quantum dots (PQDs) using *in situ* photoluminescence (PL) and absorption (Abs) spectroscopy in a mass transfer-controlled reaction

Department of Chemical and Biomolecular Engineering, North Carolina State University, Raleigh, NC 27606, USA.

E-mail: abolhasani@ncsu.edu; Web: www.abolhasanilab.com

† Electronic supplementary information (ESI) available: Supporting figures, supporting text. See DOI: 10.1039/d0re00129e

environment. Utilizing the developed flow chemistry strategy, we conducted 84 experiments to systematically investigate the relationship between ligand concentration – oleic acid (OA) – and precursor mixing time on the resulting optoelectronic properties of PQDs, all within just over 4 h and using less than 70 ml of reactants. Further applications of this device include reaction studies with homogenous reactive plugs, controlled advection rates, and arbitrarily long residence times, while requiring as little as 80 μ L of reactants per experimental condition.

The flow system, illustrated in Fig. 1, operates through a sample loop configuration on a computer-controlled six-port, two-position valve. This system can automatically pass a small sample of the reaction mixture (3.5 μ L) from the precursor mixing line (shown in green) to the sampling line (shown in gray) for downstream *in situ* analyses. The 7.4 μ L mixing line is first set to specified precursor flow rates (Q_1 and Q_2) – corresponding to a desired mixing time (t_m) and an average total flow velocity (u_m). The micromixer section equilibrates for four times the residence time from the T-junction to the sample loop. The valve is then automatically switched to redirect the reactive phase to the sampling line, filled with an inert carrier fluid, for analysis. The isolated 3.5 μ L plug is carried through the sampling flow reactor at a fluid velocity (u_r) that is set independently of u_m .

The braided tubing micromixer connected to the precursor mixing line is a facile, passive microscale mixing module for controlled and enhanced mixing of miscible fluids within a small volume. It is comprised solely of Teflon tube (fluorinated ethylene propylene, FEP) segment with an inner diameter (ID) of 250 μ m, braided in a configuration often referred to as a “chain sinnet”. Each loop was tightened to the greatest extent possible without deformation of the tubing – *i.e.*, the four-loop knot and corresponding fittings required approximately 13 cm of tubing. Such a configuration enables asymmetric switching of the fluid momentum direction, thereby enabling chaotic motion within the fluid to enhance microscale mixing rates.^{27–29} Furthermore, higher

flow velocities benefit from enhanced mixing in the T-junction before moving into the micromixer, as has been reported in prior literature.^{30,31}

In the first set of experiments, we characterized the microscale mixing performance of the braided micromixer for enhanced mixing of miscible fluids. The mixing time of two miscible fluids within the braided micromixer was measured using fluorescence quenching of fluorescein through the addition of potassium iodide (KI). A 0.75 mM solution of fluorescein was combined with a 0.5 M solution of KI in a 1:1 volumetric ratio (*i.e.*, $Q_1 = Q_2$). The PL spectra of the mixed fluid (*i.e.*, quenched fluorescein) was measured at different tubing lengths using both a braided and an unmodified straight length of Teflon tubing. Fig. 2A and B shows the measured mixing ratio (R) – see Materials and methods and ESI† section S2 – at different flow conditions and plotted as a function of the corresponding residence time (t) in the mixing line. For each Peclet number ($Pe = u_m r_m / D$, where r_m is the tube diameter and D is the diffusivity of KI in DI water),³² the measured R values were linearly fitted as a function of $\log_{10}(t)$. This empirical model is shown in eqn (1):

$$R(t) = a_0 + a_1 \log_{10}(t) \quad (1)$$

where a_0 and a_1 are fitting constants. t_m was then defined as the time at which $R(t)$ is equal to 0.1, according to eqn (2):

$$t_m = t(R(t) = 0.1) \quad (2)$$

In the occurrence that all measured R values were below 0.1, the t_m was set equal to the lowest measured t .

Calculated t_m values were then plotted in Fig. 2C according to the chaotic mixing scaling law reported in Stroock *et al.* and Song *et al.*^{9,33} The linear correlation of t_m as a function of $(r_m/u_m)\log(Pe)$ suggests a chaotic advection mixing mechanism within the braided micromixer. As expected, the control experiment (*i.e.*, straight Teflon tubing)

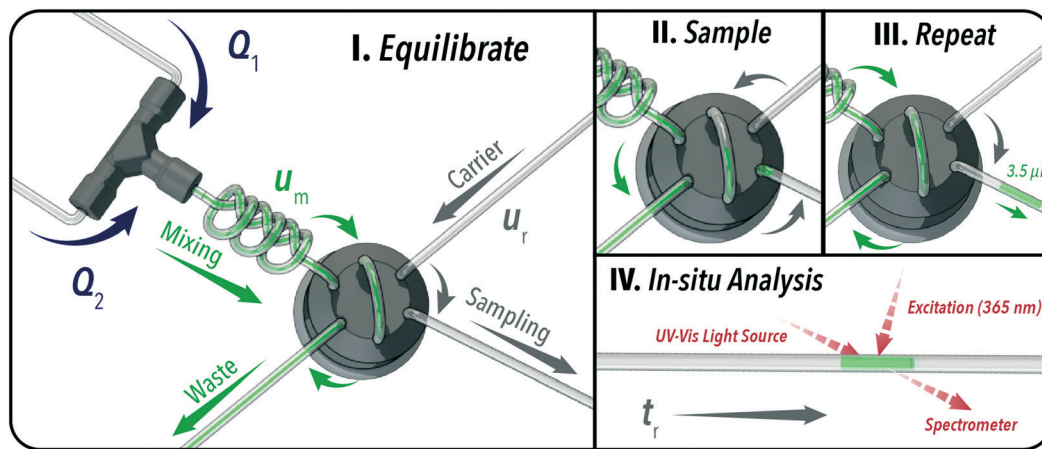


Fig. 1 Illustration of developed flow reactor for decoupling mixing and residence times with step-wise demonstration of automated system operation protocol.

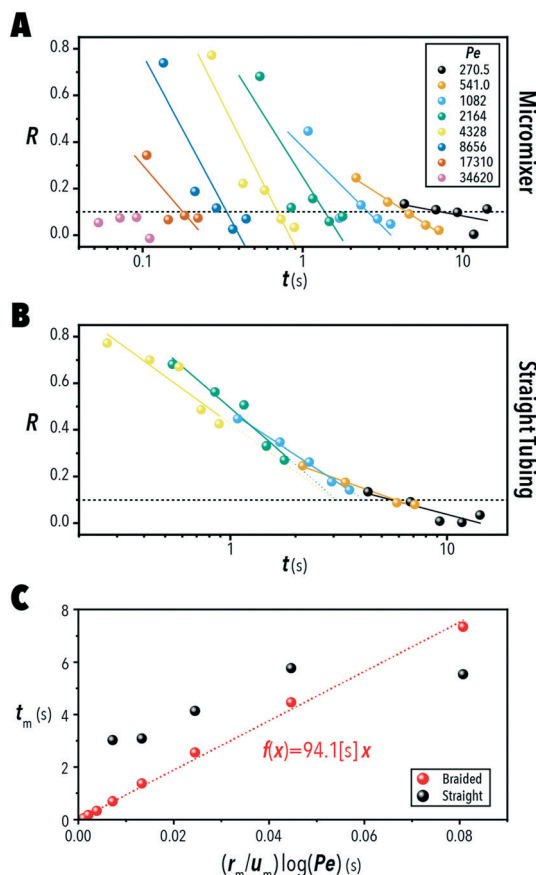


Fig. 2 Mixing ratio, R , as a function of residence time under varying Pe values for the quenching of fluorescein with KI in (A) the braided tubing micromixer and (B) an unmodified straight tubing. (C) The calculated mixing time, t_m , as a function of $(r_m/u_m)\log(Pe)$.

does not share this trend. The t_m values for proceeding synthesis studies were calculated from the correlation shown in Fig. 2C. Through these studies, the braided micromixer achieved mixing times as low as one quarter of the straight tubing control.

To demonstrate the efficacy and versatility of the developed flow chemistry, we utilized the sample loop reactor integrated with the braided mixer to investigate the ligand assisted re-precipitation synthesis of cesium lead bromide PQDs.^{16,34} Two precursor streams of cesium-lead oleate (CsPb) and tetraoctyl ammonium bromide (Br) were combined in a 1:1 volumetric ratio using varying amounts of OA. OA volume fractions were set through the injection ratio between two solutions of 1 vol% and 7.5 vol% OA prepared for both CsPb and Br precursors. The solutions of varying OA composition for each precursor stream were combined in separate braided micromixers followed by a third braided micromixer for in-flow mixing of PQD precursors before automatic sampling and *in situ* analysis – see ESI† section S3 for more information. The OA volume fraction was maintained equal between CsPb and Br precursor streams throughout this study. PL and Abs spectra of the in-flow synthesized PQDs under different precursor mixing times

were acquired *in situ* from the sampling line at a position corresponding to a 1 min residence time after the sample loop section. The residence time at the measurement point was selected to ensure complete reaction of the precursors – see ESI† section S4.^{16,34}

To first show the significance of mixing time in the synthesis of PQDs Abs and PL spectra were collected at varying t_m values and a constant OA volume fraction of 1.8 vol%. As shown in Fig. 3, varying t_m values from 0.3 s to 6.3 s, without any compositional changes to the starting precursors, produces PQDs of widely varying PL emission colors (ranging from blue to cyan to green) and bandgap energies. The results shown in Fig. 3 suggests that the precursor mixing time is one of the key parameters controlling the optoelectronic properties of colloidal QDs with fast kinetics and may provide valuable insights into the issues surrounding batch-to-batch QD variations in flask-based syntheses. Furthermore, the tunable mixing time may be applied to determining the optimal synthesis conditions of QDs with desired optoelectronic properties for targeted applications in photonic devices. As a demonstration of this principal, we systematically studied the effect of varying the volumetric fraction of OA (ϕ_{OA}) from 1.8 to 6.7 vol% on the

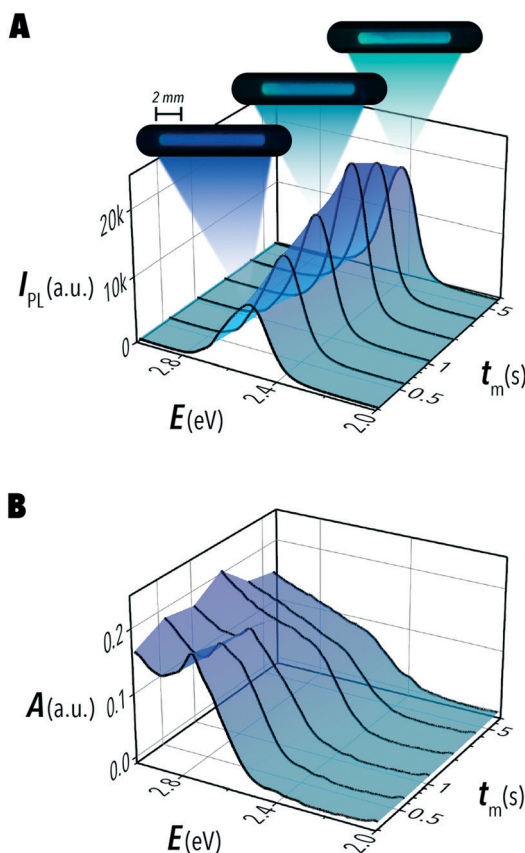


Fig. 3 (A) PL spectra with sample fluorescence images of corresponding PQD plugs under UV illumination, and (B) their corresponding Abs spectra for PQDs synthesized under six different t_m values with a constant OA concentration of 1.8 vol%.

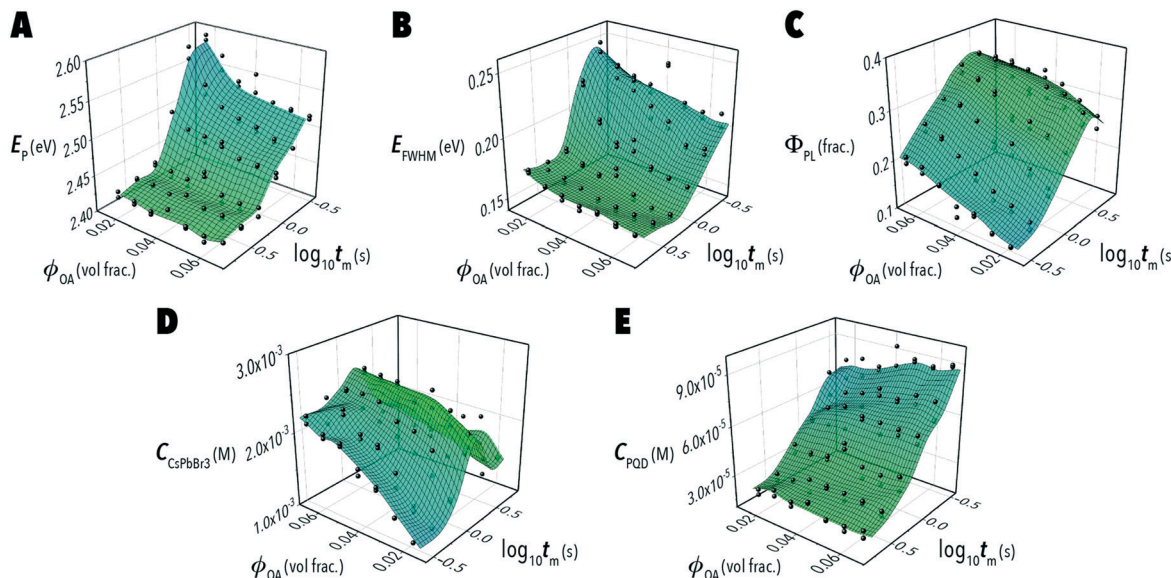


Fig. 4 (A) Peak emission energy, (B) emission full-width at half-maximum, (C) photoluminescence quantum yield, (D) molar concentration of CsPbBr_3 , and (E) nanoparticle concentration of CsPbBr_3 quantum dots as a function of OA concentration and mixing time for 42 reaction conditions with one replicate each at a residence time of 1 min. Surface meshes are derived using a cubic interpolant fit of the experimental data and colored corresponding to the measured peak emission energy.

PQD optical properties across the same t_m values (a total of 84 automated experiments).

Fig. 4 shows the complex PQDs reaction space associated with ϕ_{OA} and t_m derived utilizing the automated flow chemistry platform developed in this study. As shown in Fig. 4A, the peak emission energy (E_p) of in-flow synthesized PDQs has a stronger dependence on ϕ_{OA} at higher t_m values; however, mass transfer and ligand concentration effects on E_p plateau for t_m greater than 1.9 s. In the search for the highest quality PQDs (Fig. 4B and C), the in-flow synthesized PQDs with slower precursor injection rates (*i.e.*, lower mixing rates) generally outperform the higher advection rate experiments in terms of emission full-width at half-maximum (E_{FWHM}) and photoluminescence quantum yield (Φ_{PL}). However, after the PQD precursor mixing time surpasses approximately 3.5 s, the resulting reaction yield and Φ_{PL} begin to decrease while the polydispersity increases (Fig. 4B-D). Furthermore, decoupling the precursor mixing time and overall reaction time of colloidal PQDs provides valuable insights into the formation and growth mechanisms of perovskite nanocrystals. As shown in Fig. 4D and E, the concentrations of CsPbBr_3 (C_{CsPbBr_3}), derived from the *in situ* Abs spectra, indicate that higher mixing rates and lower OA concentrations both contribute to a less efficient consumption of available precursors. When the molar concentration of QD nanocrystals (C_{PQD}) is considered, more nanocrystals are formed at higher precursor mixing rates and higher OA concentrations.

The case study results presented in Fig. 3 and 4, show the capabilities of the developed flow chemistry platform in exploring the influences of precursor mixing times on the optoelectronic properties of colloidal nanocrystals. Utilizing

this modular flow chemistry platform could therefore unlock higher quality PQDs under replicable synthesis conditions amenable to continuous manufacturing. It should be noted that more extensive characterization of mass transfer within the flow reactor is required before reaction conditions may be transferred to a continuous manufacturing process. Furthermore, more advanced sampling techniques are necessary for studying the influences of synthesis temperature. Despite these limitations, we believe the developed flow chemistry strategy has immediate applications in fundamental and applied studies of a wide range of solution-phase chemical processes. Notably, no portion of the flow chemistry platform is reliant on custom-machined components and requires little specialized knowledge in its assembly. It is therefore highly accessible to users spanning a wide range of research fields from organic/inorganic synthesis to colloidal nanoscience.

Materials and methods

Precursor preparation

The fluorescein solution for studies of microscale mixing time was prepared by mixing 5 mg of fluorescein with 80 mg of sodium hydroxide and 20 mL of deionized (DI) water. The KI quenching solution was prepared by mixing 1.66 g of KI with 20 mL of DI water.

The stock solution of CsPb precursor (1 M) was prepared by mixing 443 mg of lead oxide, 172.4 μL of cesium hydroxide solution, and 2 mL of OA in an 8 mL ventilated vial. While stirring, the contents were heated in an oil bath at 160 °C for 1 h then moved to an oven at 120 °C for 1 h. The 1% OA-CsPb precursor was prepared by combining 0.4 mL of the 1

M solution with 39.6 mL of toluene in a 40 mL vial. The 7.5% OA-CsPb precursor was formed similarly by combining 0.4 mL of 1 M solution, 2.6 mL of OA, and 37 mL of toluene.

The 0.01 M Br precursors were prepared by adding 218 mg of tetraoctylammonium bromide to two 40 mL vials. The 1% and 7.5% OA-Br precursors were prepared by adding 0.4 mL and 3.0 mL of OA, respectively to toluene to total 40 mL each.

Flow reactor operation

Automated flow synthesis was conducted using a central control algorithm integrated with five syringe pumps, a two-position six-port valve, a fiber-coupled UV-vis spectrometer, a deuterium-halogen light source, and a high power light-emitting diode (LED) (365 nm). Flow synthesis experimentation was performed by first setting the flow rates of the four precursor pumps and the PFO pump with the sample loop segment open to the PFO fluidic line, then the system was allowed to equilibrate for 1 min. Next, the sample loop was switched to the precursor fluidic line for 10 s, followed by returning to the PFO fluidic line for 6 s. This process was repeated three more times to produce four total reactive plugs at each desired precursor mixing time.

Spectral sampling was then carried out with a three-port optical flow cell^{18,35} by alternating between the light source and LED with continuous sampling every 25 ms for 5 s each. This process was repeated five times for a total of 2000 PL and Abs spectra per sample. The reactive phase in these data sets was isolated using the protocol detailed in Epps *et al.*,¹⁶ and empty intervals were discarded.

Mixing correlations

The Peclet number for each flow velocity was calculated using eqn (3),

$$Pe = r_m u_m / D \quad (3)$$

where diffusivity D was estimated as 1.90×10^{-5} cm s⁻¹ for KI in water according to Dunlop *et al.*, and 2.13×10^{-5} cm s⁻¹ for bromine in toluene according to the Stokes-Einstein relationship and ion properties detailed in Krall *et al.*^{32,36}

The mixing ratio R used in fluorescein quenching studies was defined according to the relationship

$$R = (I_S - I_Q) / (I_U - I_Q) \quad (4)$$

where I represents the peak intensity of the PL spectra and subscripts S , Q , and U correspond to the *in situ* flow measurements on the mixing system, the fully quenched fluorescein reference, and the unquenched fluorescein reference, respectively.

PQD property calculations

Relative Φ_{PL} of the in-flow synthesized PQDs was calculated using a solution of quinine sulfate in 0.05 M sulphuric acid.

See ESI† section S5. Nanoparticle concentrations of CsPbBr₃ and the molar concentrations of PQDs were calculated from the Abs spectra according to the intrinsic absorption coefficient and molar extinction coefficients along with the correlations detailed in Maes *et al.* and De Roo *et al.*^{37,38} Nanocrystal edge lengths for these calculations were estimated according to the relationship with peak emission energy demonstrated in Protesescu *et al.*³⁹ See ESI† section S6 for detailed calculations.

Data availability

All presented experimental data is available upon request.

Conflicts of interest

There are no conflicts to declare.

Acknowledgements

The authors gratefully acknowledge the financial support provided by the National Science Foundation (Award # 1902702) and the UNC Research Opportunities Initiative (UNC-ROI) grant and North Carolina State University.

References

1. J. Yoshida, A. Nagaki and T. Yamada, *Chem. – Eur. J.*, 2008, **14**, 7450–7459.
2. H. Song and R. F. Ismagilov, *J. Am. Chem. Soc.*, 2003, **125**, 14613–14619.
3. K. S. Elvira, X. C. I. Solvas, R. C. R. Wootton and A. J. deMello, *Nat. Chem.*, 2013, **5**, 905–915.
4. B. K. H. Yen, A. Günther, M. A. Schmidt, K. F. Jensen and M. G. Bawendi, *Angew. Chem., Int. Ed.*, 2005, **44**, 5447–5451.
5. L. Bezinge, R. M. Maceczky, I. Lignos, M. V. Kovalenko and A. J. deMello, *ACS Appl. Mater. Interfaces*, 2018, **10**, 18869–18878.
6. A. M. Nightingale, J. H. Bannock, S. H. Krishnadasan, F. T. F. O'Mahony, S. A. Haque, J. Sloan, C. Drury, R. McIntyre and J. C. deMello, *J. Mater. Chem. A*, 2013, **1**, 4067–4076.
7. J. P. McMullen and K. F. Jensen, *Annu. Rev. Anal. Chem.*, 2010, **3**, 19–42.
8. S. Marre and K. F. Jensen, *Chem. Soc. Rev.*, 2010, **39**, 1183–1202.
9. A. D. Stroock, S. K. W. Dertinger, A. Ajdari, I. Mezić, H. A. Stone and G. M. Whitesides, *Science*, 2002, **295**, 647–651.
10. K. Wang, H. Zhang, Y. Shen, A. Adamo and K. F. Jensen, *React. Chem. Eng.*, 2018, **3**, 707–713.
11. P.-H. Huang, Y. Xie, D. Ahmed, J. Rufo, N. Nama, Y. Chen, C. Y. Chan and T. J. Huang, *Lab Chip*, 2013, **13**, 3847–3852.
12. M. Abolhasani, E. Kumacheva and A. Günther, *Ind. Eng. Chem. Res.*, 2015, **54**, 9046–9051.
13. A. Günther, S. A. Khan, M. Thalmann, F. Trachsel and K. F. Jensen, *Lab Chip*, 2004, **4**, 278–286.
14. J. Tan, Y. C. Lu, J. H. Xu and G. S. Luo, *Chem. Eng. J.*, 2012, **181–182**, 229–235.

15 J. D. Tice, H. Song, A. D. Lyon and R. F. Ismagilov, *Langmuir*, 2003, **19**, 9127–9133.

16 R. W. Epps, K. C. Felton, C. W. Coley and M. Abolhasani, *Lab Chip*, 2017, **17**, 4040–4047.

17 K. Abdel-Latif, R. W. Epps, C. B. Kerr, C. M. Papa, F. N. Castellano and M. Abolhasani, *Adv. Funct. Mater.*, 2019, **29**, 1900712.

18 R. W. Epps, K. C. Felton, C. W. Coley and M. Abolhasani, *J. Visualized Exp.*, 2018, e57666.

19 M. Abolhasani, C. W. Coley, L. Xie, O. Chen, M. G. Bawendi and K. F. Jensen, *Chem. Mater.*, 2015, **27**, 6131–6138.

20 M. Abolhasani and K. F. Jensen, *Lab Chip*, 2016, **16**, 2775–2784.

21 M. Abolhasani, N. C. Bruno and K. F. Jensen, *Chem. Commun.*, 2015, **51**, 8916–8919.

22 C. Zhu, K. Raghuvanshi, C. W. Coley, D. Mason, J. Rodgers, M. E. Janka and M. Abolhasani, *Chem. Commun.*, 2018, **54**, 8567–8570.

23 R. J. Sullivan and S. G. Newman, *J. Org. Chem.*, 2020, **85**, 5464–5474.

24 C. W. Coley, M. Abolhasani, H. Lin and K. F. Jensen, *Angew. Chem.*, 2018, 9847–9850.

25 F. Gielen, L. van Vliet, B. T. Koprowski, S. R. A. Devenish, M. Fischlechner, J. B. Edel, X. Niu, A. J. deMello and F. Hollfelder, *Anal. Chem.*, 2013, **85**, 4761–4769.

26 M. E. Dolega, S. Jakiela, M. Razew, A. Rakszewska, O. Cybulski and P. Garstecki, *Lab Chip*, 2012, **12**, 4022–4025.

27 Y. Lin, *Chem. Eng. J.*, 2015, **277**, 303–311.

28 R. H. Liu, M. A. Stremler, K. V. Sharp, M. G. Olsen, J. G. Santiago, R. J. Adrian, H. Aref and D. J. Beebe, *J. Microelectromech. Syst.*, 2000, **9**, 190–197.

29 G. Cai, L. Xue, H. Zhang and J. Lin, *Micromachines*, 2017, **8**, 274.

30 M. A. Ansari, K.-Y. Kim and S. M. Kim, *Micromachines*, 2018, **9**, 204.

31 V. Hessel, H. Löwe and F. Schönfeld, *Chem. Eng. Sci.*, 2005, **60**, 2479–2501.

32 P. J. Dunlop and R. H. Stokes, *J. Am. Chem. Soc.*, 1951, **73**, 5456–5457.

33 H. Song, M. R. Bringer, J. D. Tice, C. J. Gerdts and R. F. Ismagilov, *Appl. Phys. Lett.*, 2003, **83**, 4664–4666.

34 S. Wei, Y. Yang, X. Kang, L. Wang, L. Huang and D. Pan, *Chem. Commun.*, 2016, **52**, 7265–7268.

35 C. B. Kerr, R. W. Epps and M. Abolhasani, *Lab Chip*, 2019, **19**, 2107–2113.

36 A. H. Krall, J. V. Sengers and J. Kestin, *J. Chem. Eng. Data*, 1992, **37**, 349–355.

37 J. Maes, L. Balcaen, E. Drijvers, Q. Zhao, J. De Roo, A. Vantomme, F. Vanhaecke, P. Geiregat and Z. Hens, *J. Phys. Chem. Lett.*, 2018, **9**, 3093–3097.

38 J. De Roo, M. Ibáñez, P. Geiregat, G. Nedelcu, W. Walravens, J. Maes, J. C. Martins, I. Van Driessche, M. V. Kovalenko and Z. Hens, *ACS Nano*, 2016, **10**, 2071–2081.

39 L. Protesescu, S. Yakunin, M. I. Bodnarchuk, F. Krieg, R. Caputo, C. H. Hendon, R. X. Yang, A. Walsh and M. V. Kovalenko, *Nano Lett.*, 2015, **15**, 3692–3696.